Proteins in hydrothermal carbonization liquor of sewage sludge interfere with vivianite crystallization for phosphorus recovery

Zhang, Yue; Yang, Xiaofan; Zhang, Xinran; Sun, Dezhi; Liu, Xinyi; Lan, Rui; Zheng, Min; van Loosdrecht, Mark C.M.; Cheng, Xiang

DOI
10.1016/j.resconrec.2024.107731

Publication date
2024

Document Version
Final published version

Published in
Resources, Conservation and Recycling

Resources, Conservation & Recycling 208 (2024) 107731

Contents lists available at ScienceDirect

Resources, Conservation & Recycling

journal homepage: www.sciencedirect.com/journal/resources-conservation-and-recycling

Full length article

Proteins in hydrothermal carbonization liquor of sewage sludge interfere with vivianite crystallization for phosphorus recovery

Yue Zhang [a], Xiaofan Yang [a], Xinran Zhang [a], Dezhi Sun [a], Xinyi Liu [a], Rui Lan [a], Min Zheng [b], Mark C.M. van Loosdrecht [c], Xiang Cheng [a,*]

[a] Beijing Key Laboratory for Source Control Technology of Water Pollution, Beijing Forestry University, Beijing 100083, China
[b] Water Research Centre, School of Civil and Environmental Engineering, University of New South Wales, Sydney, NSW 2052, Australia
[c] Department of Biotechnology, Delft University of Technology, van der Maasweg 9, 2629 HZ, Delft, the Netherlands

ARTICLE INFO

Keywords:
Sludge carbonization
Vivianite
Crystal growth
Phosphorus
Protein

ABSTRACT

Hydrothermal carbonization (HTC) liquor of waste activated sludge generated during urban sewage biotreatment contains high concentrations of phosphate and thus is an appropriate resource for phosphorus recovery. The influence of proteins in the HTC liquor on vivianite crystallization, as a promising phosphorus recovery method, was investigated in this study from the perspectives of removal efficiencies and product properties. The proteins in the HTC liquor were observed to remain in unhydrolyzed forms with free amino acids having a negligible concentration. For vivianite crystallization in the synthetic HTC liquor with bovine serum albumin (BSA) mimicking the unhydrolyzed proteins, the efficiencies of phosphorus removal and crystallization at pH 6 decreased by 13.5 % and 18.4 %, respectively, compared with the BSA-free controls. The strong interaction between Fe and the proteins was suggested to be responsible for the reduced efficiency of vivianite formation and the variation of crystal growth mode from spirally expanding to *x/z*-axis extending.

1. Introduction

Phosphorus (P) is an essential and irreplaceable element for all living organisms whilst is hardly renewable under current technological conditions (Mew, 2016; Steiner and Geissler, 2018). In recent years, the massive consumption of phosphorus resources without effective recovery and reuse has led to fast reduction in the phosphate rock reserves (Cordell et al., 2009). The global loss of phosphorus resources to freshwater was estimated to be 9–14 Mt a-1 (Brownlie et al., 2021). It is also reported that 22 % of world demand for phosphate rock could be met by merely recycling phosphorus in human wastes (Chrispim et al., 2019).

Urban sewage contains approximately 3–5 mg L^{-1} of phosphorus (King et al., 1983), most of which will be enriched in waste activated sludge during the biochemical treatments in wastewater treatment plants (Yu et al., 2021). Sludge reduction, treatment and utilization have become mandatory in many countries to minimize its potential environmental impact (Kelessidis and Stasinakis, 2012; Yang et al., 2015). Among the sludge treatment technologies, hydrothermal carbonization (HTC) has attracted increasing attention because of its potentials in facilitating waste sludge reduction and nutrients recovery (Huang et al., 2018; Wang et al., 2019; Xu et al., 2020). At a hydrothermal temperature of < 250 °C, the sludge is decomposed and is subsequently converted into a solid with a wide range of resources (Khalaf et al., 2023). HTC eliminates the need for sludge drying as a pretreatment step, allowing for effective treatment even when the sludge has a high moisture content. During the HTC process, most of the sludge phosphorus would end up in inorganic forms (Huang et al., 2017). Organophosphate compounds, polyphosphates and pyrophosphates can be converted into orthophosphates with a considerable proportion (e.g., 49 %) being solubilized in the liquid phase (Huang and Tang, 2015; Lühmann and Wirth, 2020; Ovsyannikova et al., 2019; Shi et al., 2019; Aragón-Briceño et al., 2021). As such, the resulting stream contains a large amount of orthophosphate which is relatively easy to recover. However, because of the complex nature of HTC liquor, such as the highly diverse organic components that are difficult to identify and quantify (Xu et al., 2022), methods for effectively recovering the enriched phosphorus need to be developed.

As direct reuse of phosphorus-carrying waste streams and solids to agriculture has been banned in most countries (Karunanithi et al., 2015;

* Corresponding author.
E-mail address: xcheng@bjfu.edu.cn (X. Cheng).

https://doi.org/10.1016/j.resconrec.2024.107731
Received 14 February 2024; Received in revised form 29 April 2024; Accepted 24 May 2024
Available online 30 May 2024

Senthilkumar et al., 2014), phosphate crystallization is believed to be a practical option for phosphorus recovery with the products including calcium phosphates, struvite and vivianite (Liu et al., 2021; Wang et al., 2022; Zhang et al., 2020). Recently, crystallization of vivianite ($3Fe^{2+} + 2PO_4^{3-} + 8H_2O \rightarrow Fe_3(PO_4)_2{\cdot}8H_2O$) has attracted particular attention due to the circumneutral working pH and the cost effectiveness by using inexpensive Fe^{2+} salts (Wu et al., 2019; Wilfert et al., 2016). Priambodo et al. (2017) employed a fluidized bed crystallizer to treat phosphorus-rich wastewater generated during the manufacture of thin film transistor-liquid crystal displays, and proved that a phosphorus removal efficiency of 95 % with a crystallization ratio of 63 % was achieved via vivianite formation under the optimized operating condition. From the perspective of thermodynamics, the vivianite pathway of phosphate recovery was reported to be compatible with the conditions in anaerobic sludge digestion systems (Liu et al., 2018). In fact, the formation of vivianite has been observed in the activated sludge in multiple locations, such as surplus sludge lines and anaerobic digesters (Prot et al., 2021; Wilfert et al., 2016). The formation and stable presence of vivianite crystals was also reported in wastewater biotreatment systems even with aerobic units (Deng et al., 2020). Additionally, in a membrane bioreactor for the acidogenic co-fermentation of activated sludge and food waste, effective recovery of phosphorus was reported in the form of vivianite (Li et al., 2018).

For the real application of vivianite crystallization to recover phosphorus from HTC liquor, understanding of the influencing factors is important for process optimization. Several recent studies have discussed the key factors influencing vivianite formation, such as pH and dissolved oxygen (DO) (Gächter and Müller, 2003; Liu et al., 2018). The carbonization liquor generated during the HTC treatment of waste sludge contains not only high concentrations of phosphorus but also a considerable amount of organic compounds, including proteins as the most abundant organic molecules in microbial cells (Huang et al., 2021). It was observed that natural organic matter readily binds Fe^{II} under circumneutral reducing conditions, forming primarily mononuclear complexes with citrate-like groups (Daugherty et al., 2017). However, the influence of organic matters, especially proteins on vivianite formation has not been clarified. As macromolecules with a complex spatial structure, proteins may strongly interact with Fe^{II} by forming organic-Fe^{II} complexes (Qiao and Xie, 2019), reducing the availability of Fe^{II} for vivianite crystallization (Chen et al., 2022).

The aim of this study was to explore the influences of proteins in the HTC liquor on vivianite crystallization for phosphorus recovery. Crystallization experiments were conducted with proteins and the monomers, i.e., the component amino acids, to discuss the mechanisms of protein-interfered vivianite crystallization.

2. Materials and methods

2.1. Chemicals and HTC liquor

All the inorganic and organic chemicals were of analytical reagent grade. The inorganic chemicals were purchased from Guangfu Co., Ltd (Tianjin, China). The amino acids were purchased from Meryer Chemical Technology Co., Ltd (Shanghai, China). The bovine serum albumin (BSA, lyophilized powder, V900933) was purchased from Sigma-Aldrich (St. Louis, USA).

The sample of HTC liquor of waste sludge was from Jinzhong wastewater treatment plant in Shanxi, China. The HTC liquor was generated during the carbonization of waste sludge with 80 % moisture content under the conditions of <300 °C and <10 Mpa. The water quality of the HTC liquor is detailed in Table S1. A phosphate solution of 4.13 mM, as synthetic HTC liquor, was prepared with Na_2HPO_4 and NaH_2PO_4 according to the measured concentration of PO_4-P in the real HTC liquor. Four thousand mg/L of BSA was added to the solution to mimic the proteins in the HTC liquor. The synthetic HTC liquor was also amended with glutamic acid (2.15 mM), alanine (2.71 mM), glycine (2.97 mM), phenylalanine (0.66 mM), methionine (0.32 mM) or histidine (0.18 mM) in the experiments for studying the influences of these individual amino acids. A concentrated Fe^{2+} solution of 123.9 mM, prepared by using $FeSO_4{\cdot}7H_2O$, was used to add Fe^{2+} for the vivianite crystallization experiments.

All the solutions for crystallization experiments and water sample analyses in this study were prepared with oxygen-removed deionized (DI) water in order to minimize the oxidation of ferrous ions. The DO levels were below the detection limit, namely 2 %, of the Oxi3310 DO meter (WTW, Germany) after the solutions were purged with high-purity N_2 gas.

2.2. Crystallization experiments

Vivianite crystallization experiments were conducted in a tightly sealed continuous stirred-tank reactor with a working volume of 550 mL (Fig. S1). To minimize Fe^{II} oxidation, aluminum foil was used to wrap the reactor and the Fe^{II} solution flask to protect them from light exposure during the entire experiment. The hydraulic retention time (HRT) was 30 min by adjusting the flow rate of synthetic HTC liquor as the feed. An Fe^{II} solution was introduced to the reactor for an Fe/P molar ratio of 1.5 as in the formula of vivianite. The Fe^{II} solution was acidified to pH 2 to minimize Fe^{II} oxidation before being added to the reactor. The top space of the flasks of feed and Fe^{II} solution was connected to high-purity N_2 gas bags to maintain oxygen-free conditions during the experiment. Six amino acids (glutamic acid, alanine, glycine, phenylalanine, methionine and histidine), selected by considering the abundance and structure of the component amino acids of proteins in the HTC liquor, and BSA were added in the feed to study the influences of proteins on the crystallization of vivianite.

The experiment was conducted at pH 6 for efficiently recovering phosphorus whilst keeping the alkali dosage relatively small for the maintenance of pH according to previous studies (Lemos et al., 2007; Martin et al., 2020). The pH maintenance was achieved by adding 1 M NaOH continuously with a pH meter monitoring (PHS-3G, Leici, China). The concentrations of aqueous Fe^{II}, Fe^{tot} and PO_4-P were followed for 50 h (100 HRTs) till a steady state was reached. Both sampling and measurement were conducted in triplicates.

Aqueous species were measured after filtering the samples through 0.22-μm polyethersulfone membranes (Membrana, Germany). The unfiltered samples, after being treated in 3 M HCl, were used to determine the total amounts of Fe and phosphorus (including the aqueous and solid forms) in the mixture. Aqueous fractions and the total amounts were labeled with "$_{aq}$" and "$_{mx}$", respectively. During the experiment, solid samples were collected from the reactor at different operating times and were freeze-dried for further characterization.

2.3. Analyses and calculations

Concentrations of amino acids in the real HTC liquor were determined by a Hitachi amino acid analyzer (L-8900, Japan). Protein concentrations were analyzed by Folin-lowry method (Lowry et al., 1951). Concentrations of PO_4-P, Fe^{tot} ($Fe^{II} + Fe^{III}$) and Fe^{II} were measured by Hach reagent kits with a DR3900 spectrophotometer (Hach, USA). The morphology of the precipitates was analyzed using a high-resolution field emission scanning electron microscope (JSM-6700F, JEOL, Japan). The mineral phase was analyzed by a powder X-ray diffractometer (XRD-7000, Japan) in the 2θ range of $5°-80°$. Particle size distribution (PSD) was determined on a Malvern Master Sizer 3000 (U. K.). Approximately 5 ml of vivianite-containing suspension collected from the crystallization reactor was dispersed in 400 ml of oxygen-eliminated DI water at room temperature. Size distribution was quantified at 3500 rpm with each sample measured 5 times for an average.

The efficiency of phosphorus removal (E_{RM}) was used to evaluate the performance of the reactor in reducing phosphorus in the aqueous

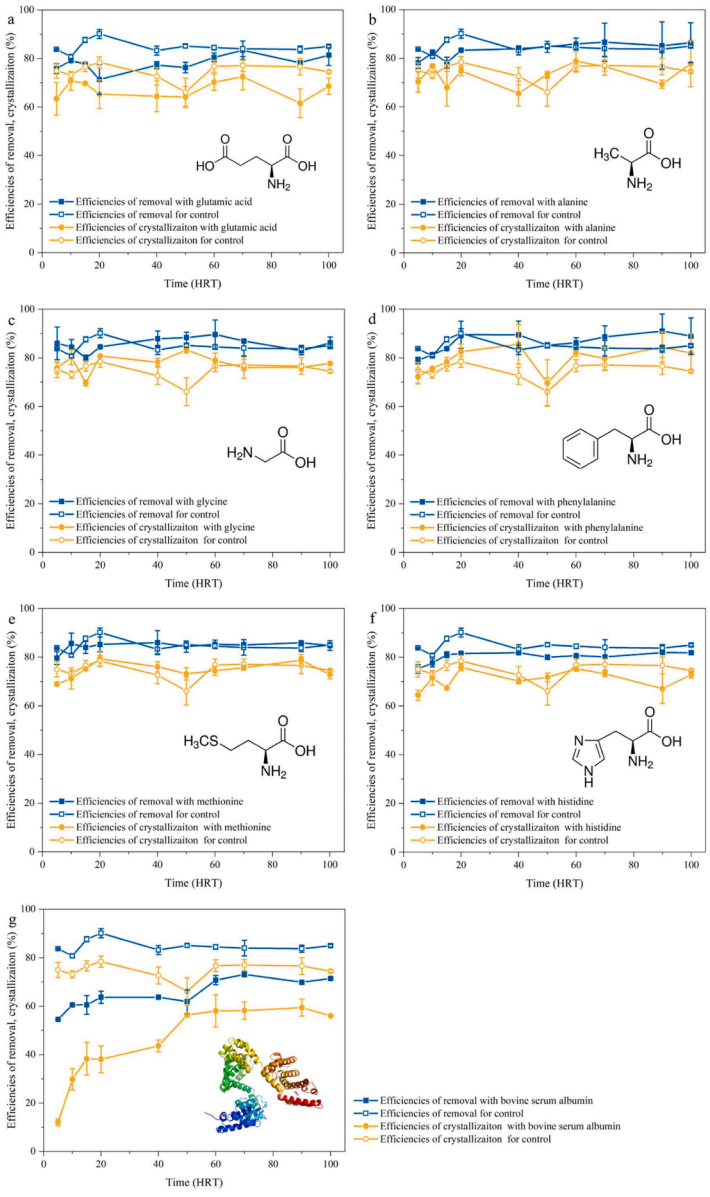

Fig. 1. Influences of bovine serum albumin and the six component amino acids on efficiencies of phosphate removal and crystallization during vivianite crystallization experiments (a: glutamic acid; b: alanine; c: glycine; d: phenylalanine; e: methionine; f: histidine; g: bovine serum albumin).

phase, while the efficiency of crystallization (E_{RC}) refers to the recoverability of the formed vivianite (excluding those washed-out fines). The two efficiencies were calculated by Eqs. (1) and (2), respectively (Yang et al., 2023).

$$E_{RM} = \frac{\left[PO_4 - P_{aq}\right]_{inf} \times Q_{inf} - \left[PO_4 - P_{aq}\right]_{eff} \times Q_{eff}}{\left[PO_4 - P_{aq}\right]_{inf} \times Q_{inf}} \quad (1)$$

$$E_{RC} = \frac{\left[PO_4 - P_{aq}\right]_{inf} \times Q_{inf} - \left[PO_4 - P_{mx}\right]_{eff} \times Q_{eff}}{\left[PO_4 - P_{mx}\right]_{inf} \times Q_{inf}} \quad (2)$$

where $[PO_4\text{-}P_{aq}]_{inf}$ and $[PO_4\text{-}P_{aq}]_{eff}$ are the concentrations of aqueous PO_4-P in the influent and effluent, respectively; $[PO_4\text{-}P_{mx}]_{eff}$ is the concentration of total amounts of PO_4-P in the effluent; Q_{inf} is the flow rate of the phosphate-containing influent; Q_{eff} is the flow rate of the effluent, equaling to the sum of Q_{inf} and Q^{II}_{Fe} (the flow rate of added Fe^{II} solution).

The degree of Fe^{II} oxidation during the reaction was determined by the mass fraction of Fe^{III} within Fe^{tot}, i.e., $m(Fe^{III})/m(Fe^{tot})$. The calculation of the mass of Fe (Fe^{III} or Fe^{tot}) include the amounts of Fe that remained in the reactor and that had been discharged via the effluents as shown in Eqs. (3) and (4) (Yang et al., 2023).

$$m\left(Fe^{III}_{mx}\right) = Q_{eff} \times \int_0^t \left[Fe^{III}_{mx}\right]_{eff} dt + V_{reac} \times \left[Fe^{III}_{mx}\right]_{reac} \quad (3)$$

$$m\left(Fe^{tot}_{mx}\right) = Q_{eff} \times \int_0^t \left[Fe^{tot}_{mx}\right]_{eff} dt + V_{reac} \times \left[Fe^{tot}_{mx}\right]_{reac} \quad (4)$$

where t is the reaction time and the Fe in the reactor is labeled with "reac".

The degree of supersaturation for vivianite in the reactor was evaluated by saturation index (SI) as can be calculated by Eq. (5).

$$SI = \log\left(\frac{IAP}{K_{sp}}\right) \quad (5)$$

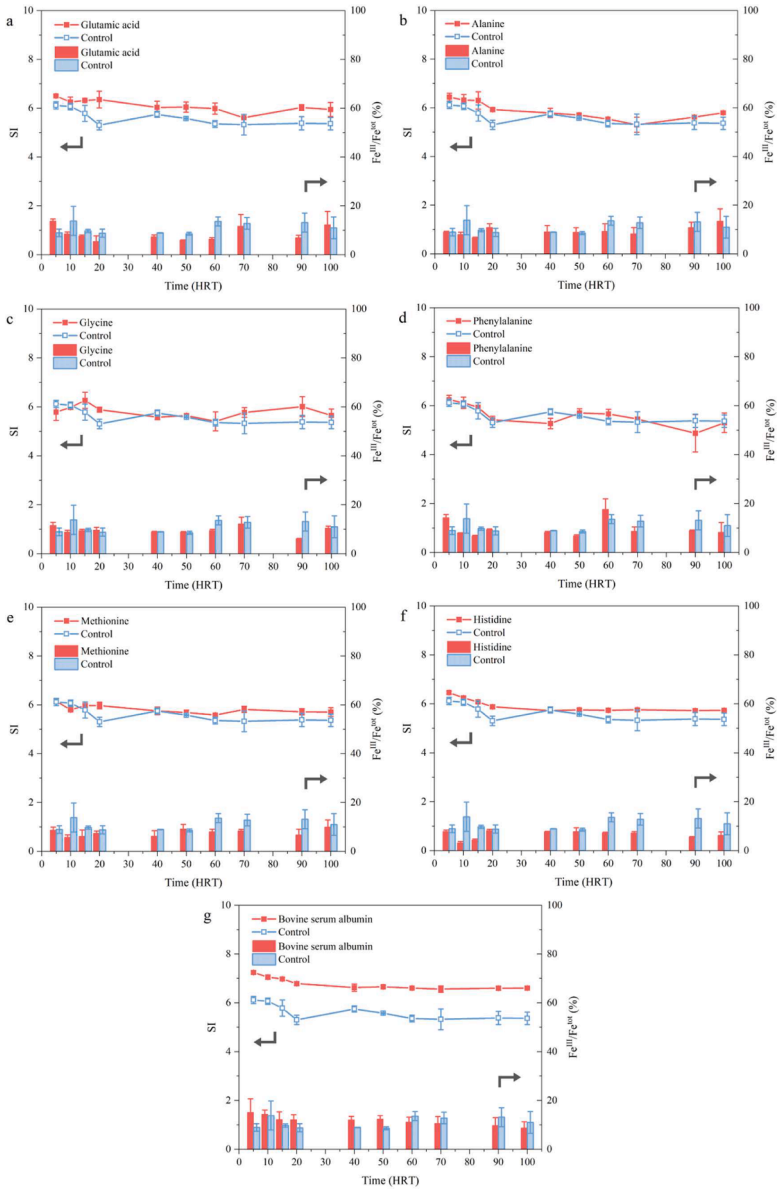

Fig. 2. Influences of bovine serum albumin and the six component amino acids on SI and Fe^{II} oxidation ratio during vivianite crystallization (a: glutamic acid; b: alanine; c: glycine; d: phenylalanine; e: methionine; f: histidine; g: bovine serum albumin).

where IAP is the activity product of ions, namely, $\{Fe^{2+}\}^3 \bullet \{PO_4^{3-}\}^2$; K_{sp} is the solubility product. The activities of Fe^{2+} and PO_4^{3-} ions and SI values were determined using Visual MINTEQ 3.0.

3. Results and discussion

3.1. Influences of proteins and amino acids on vivianite crystallization

In the HTC liquor, the proteins were observed to remain in unhydrolyzed forms with the free amino acids present in low concentrations (Table S2). After hydrolyzing the proteins in the HCl solution, 17 component amino acids were detected with the most abundant three, glycine, alanine and glutamic acid, accounting for 40.4 %. This observation suggests that unhydrolyzed proteins might play an important role in the crystallization of vivianite from the HTC liquor.

In order to explore the influences of proteins and the incorporated amino acids on the process of vivianite crystallization, BSA and six of the component amino acids were added into the phosphate feed for the crystallization experiments. BSA was chosen to mimick the proteins in the HTC liquor because: (1) the proteins in the HTC liquor were fairly diverse (Fig. S2 and Table S3), none of which was in a significantly dominant level; and (2) BSA was readily available and, more importantly, its major component amino acids were consistent with the ones detected within the proteins in the HTC liquor (Table S4). The chosen six free amino acids included the three most abundant component amino acids of the proteins in the HTC liquor and three of the others with specific molecular structures, namely carbon rings and sulfur-containing R groups.

As shown in Fig. 1a–f, none of the six amino acids imposed significant influences on vivianite crystallization with glutamic acid and histidine slightly inhibiting and phenylalanine improving the reaction. In contrast, the inhibitory effect of BSA was evident. Since the concentrations of BSA and the six amino acids were all mimicking the corresponding levels for the HTC liquor proteins and the major component amino acids in BSA were included in the investigated six free ones, the significantly higher interference from the BSA in vivianite crystallization could be attributed to its structure complexity (Fig. S3). The R groups that were the same for the free amino acids and BSA were

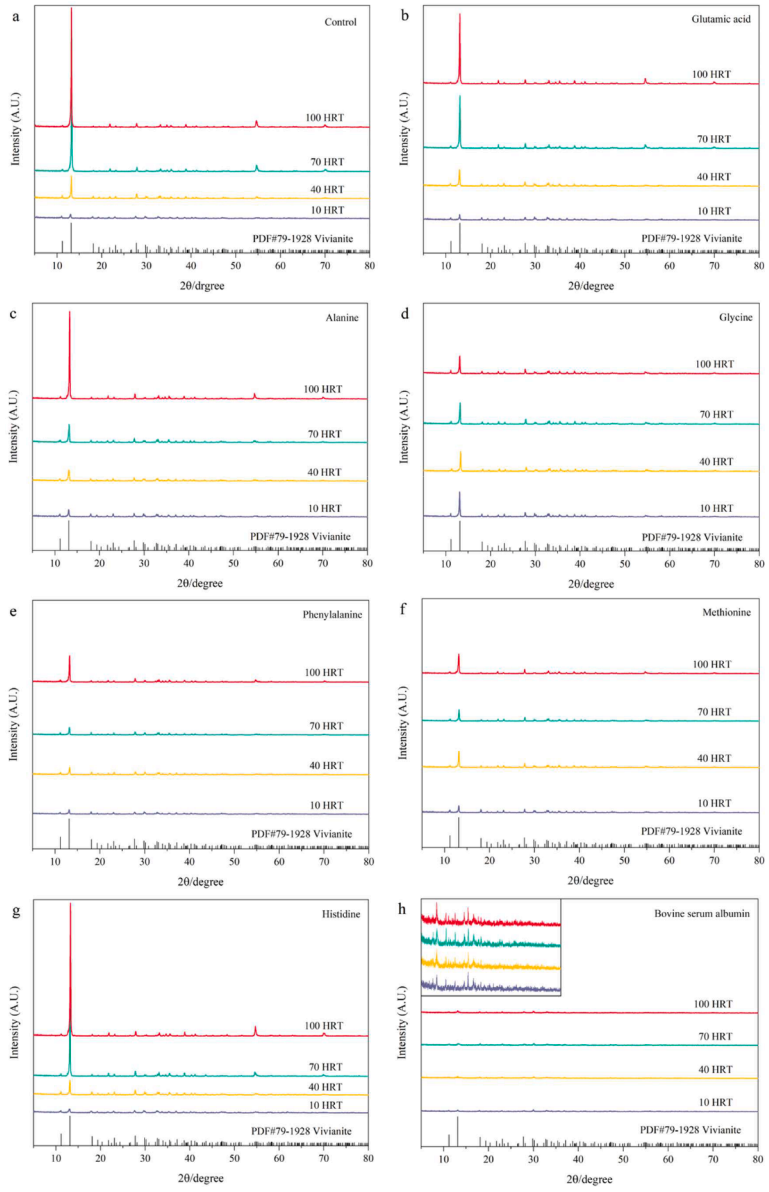

Fig. 3. XRD patterns of the obtained crystallization products in the presence of different component amino acids and bovine serum albumin (a: control; b: glutamic acid; c: alanine; d: glycine; e: phenylalanine; f: methionine; g: histidine; h: bovine serum albumin (the inset is made with a reduced scale)).

unlikely responsible for the influence of proteins on vivianite crystallization. The dehydration condensation of amino acids with the peptide bonds forming and the spatial structure resulting from the polypeptide chain folding in the proteins, could have reduced the E_{RM} and E_{RC} via vivianite crystallization. The presence of Fe in certain protein molecules, particular enzymes, has been widely recognized with the redox transformation of Fe^{II}/Fe^{III} playing an important role in transferring electrons in bioreactions (Mbughuni et al., 2010; Radisky and Kaplan, 1998). It is evident that the interaction between Fe and the multiple R groups in proteins is substantially stronger than that with individual amino acids (Albetel and Outten, 2018; Murphy et al., 2020). This would explain the observed higher interference in vivianite crystallization from BSA than the free amino acids.

3.2. *Influences of proteins and amino acids on Si and Fe^{II} oxidation*

In the crystallization reactors amended with the six amino acids, the SI levels for vivianite did not differ markedly from that in the control reactor with all the values remaining in 5–6 (Fig. 2a–f). These SI values were at the low-level side within the metastable zone, favoring the growth of vivianite crystal (Liu et al., 2018). The addition of glutamic acid led to a limited degree of increase in the SI levels during the process of vivianite crystallization. In contrast, the addition of BSA resulted in a notable increase of 1.2 in the apparent SI (the reduction in the activities of Fe^{2+} and PO_4^{3-} in the presence of proteins lack quantification methods), being ~6.6 at the stable state. Although the effects of BSA on the activities of Fe^{2+} and PO_4^{3-} are not considered in the SI calculations as the loss of free Fe^{2+} and PO_4^{3-} ions (e.g., by Fe-protein complexation) and consequently the reduction in the activity coefficients are difficult to calculate due to the structural complexity of protein molecules, it is still likely that the real SI values had shifted substantially to certain lower levels compared with those in the control and the six amino acids-amended cases. This is reflected by the larger size of vivianite crystals formed in the presence of BSA (discussed in 3.3). Also, the relatively low SI level provided a reduced driving force for vivianite crystallization and explains the reduction in both the E_{RM} and E_{RC} values in Fig. 1g, especially in the early period of the experiment.

Oxidation of aqueous Fe^{II} occurs readily when O_2 is present (Melton

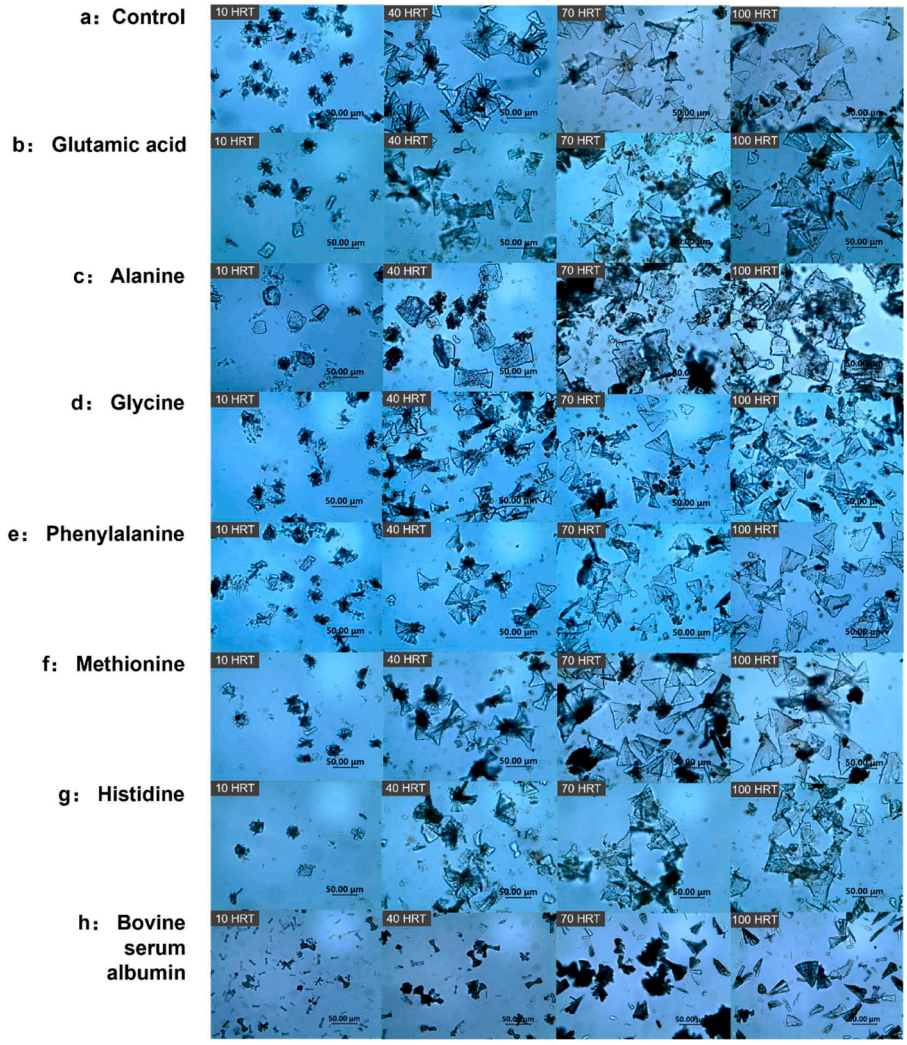

Fig. 4. Microscope images of crystallization products during 100 HRTs in the presence of different component amino acids and bovine serum albumin.

et al., 2014; Pham and Waite, 2008). Vivianite crystals were also reported to be unstable with the structural Fe^{II} being oxidized in ambient air (Chiba et al., 2020). Even in the absence of oxygen, auto-oxidation of vivianite has been observed with the production of H_2 (Hanzel et al., 1990; Pratt, 1997). Fig. 2 shows the ratios of Fe^{II} oxidation observed during the long-term operation of the crystallization reactors. Although the reactors were strictly sealed, it is found that completely avoiding Fe^{II} oxidation was impossible. The ratios of Fe^{II} oxidation under all the conditions were comparable, being in the range of 10–20 % regardless of the presence of BSA and amino acids. Therefore, in spite of the possible influence of proteins on Fe^{II} oxidation via the formation of complexes, the significant inhibition of BSA on vivianite crystallization in this study was unlikely related to the occurrence and degree of Fe^{II} oxidation which could lead to insufficiency of Fe^{II} for vivianite crystallization and formation of Fe^{III} flocs that interfere with vivianite growth, etc. (Miot et al., 2009).

3.3. *Influences of proteins and amino acids on recovered products*

The XRD patterns of the crystallization products obtained in the presence of different amino acids and BSA indicate that the recovered solids were all vivianite (PDF#79-1928) although the crystallinity differed to various extents (Fig. 3). The presence of the amino acids lowered the crystallinity of the resulting solids except for histidine, with which the crystallinity was close to that in the control reactor. The addition of BSA significantly reduced the crystallinity of the obtained vivianite, as indicated by the diffraction intensity of the major crystal planes (e.g., (020) at the 2 theta angle of 13.14°), and the crystallinity did not increase noticeably with the reaction proceeding (Fig. 3h). The results suggest that BSA in the solution inhibited the growth of vivianite crystals along the (020) plane for a flat morphology (Fig. S4).

The distinct influences of the amino acids and BSA were also evidenced by the microscopic images of the recovered products (Fig. 4). Regardless of minor variations, vivianite crystals obtained in the presence of the six amino acids were all plate-shaped, being close to the morphology of vivianite formed in the control reactors. With alanine in the solution, the crystals tended to grow to rectangular sheets (Fig. 4c), while in the presence of the other amino acids, the phosphorus products obtained were essentially single or paired triangle crystals. Interestingly, in the presence of BSA, the morphology of vivianite changed completely to be needle-shaped clusters with high uniformity (Fig. 4h). According to the XRD results, BSA interfered the mode of vivianite crystallization by inhibiting the growth along the (020) plane (Fig. 3h). This inhibition reduced the crystallization rate and consequently decreased the phosphorus removal efficiency with an increased apparent SI level (Fig. 2g) (Li and Sheng, 2021; Li et al., 2022).

The PSD curves reflect the differences in growth modes between the amino acids- and BSA-amended reaction systems (Fig. S5). The single-direction growth of vivianite in the presence of BSA resulted in big sizes and a narrower range of size distribution. In contrast, for the

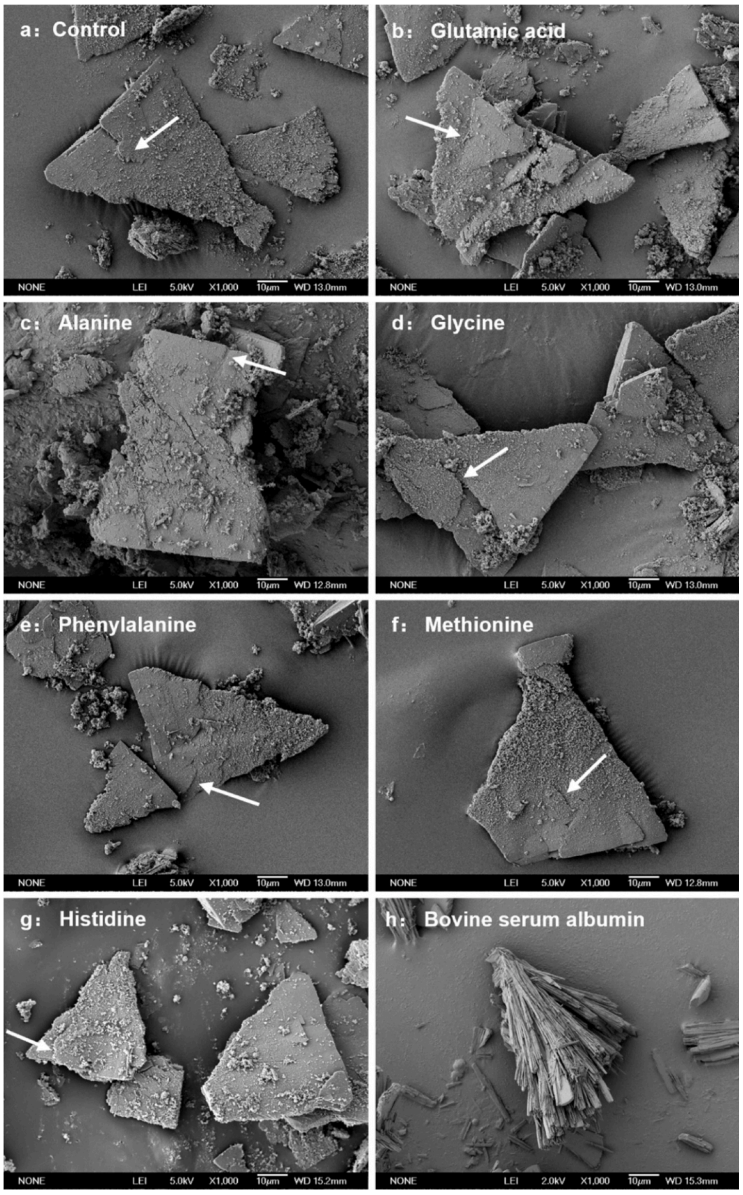

Fig. 5. SEM images of the obtained products at 100 HRTs in the presence of different amino acids and bovine serum albumin (white arrows indicate the kinks and steps observed during the spiral growth of vivianite crystals).

vivianite products obtained in the amino acids-amended solutions, the growth rates were lower with two peaks of crystal size observed, indicating a two-stage growth/aggregation mode for the crystal enlargement (insets in Fig. S5). The increased size and uniformity of products and reduced phosphorus removal efficiency for the BSA-amended system both suggest that vivianite crystallization was, indeed, proceeding at lower supersaturation levels regardless of the high values of apparent SI as a result of the incapability in quantifying the reduction in the concentrations and activities of Fe^{2+} and PO_4^{3-} ions in the presence of BSA.

The SEM images provide additional evidences for the distinct modes of vivianite growth for the amino acids- and BSA-amended systems (Fig. 5). Small amounts of floc-like materials were observed on the surface of vivianite crystals formed in the presence of the amino acids, which, according to the yellow color (observed in Fig. 4) and morphology, were likely amorphous ferric oxyhydroxide (AFO) (Mao et al., 2016). Nevertheless, the AFO did not markedly influence the spiral growth of vivianite crystals as revealed by the kinks and steps observed in Fig. 5a–g. Although the addition of BSA did not change the ratio of Fe^{II} oxidation during the crystallization (Fig. 2), it was found to have inhibited the formation of Fe^{III} flocs as seen in the amino acids-amended systems. Because of the strong Fe-BSA interaction with multiple binding sites in the protein structure and the increased apparent SI levels for vivianite formation, it is likely that the Fe^{III} from Fe^{II} oxidation had been effectively complexed to BSA (Fukuzawa et al., 2005; Hung et al., 2010). The complexation of Fe^{III} and Fe^{II} with BSA is expected to have interfered with free Fe^{2+} and PO_4^{3-} ions positioning in the kinks and steps and consequently altered the mode of vivianite growth to not expanding the plane (020) but extending along the x/z axis (Figs. 3h, 5h and S7).

Based on the above results, it is evident that the decrease in E_{RM} and E_{RC} via vivianite crystallization in the BSA-amended system is related to the structure of this protein as a macromolecule, not the individual R groups on amino acids. Although it is impossible to identify and quantify the enormous types of proteins in the HTC liquor, the strong interactions (e.g., complexation) between the proteins and Fe (including Fe^{II} and Fe^{III}) are expected (Chen et al., 2022). The Fe-protein interactions lowered the supersaturation levels by reducing the concentration of free

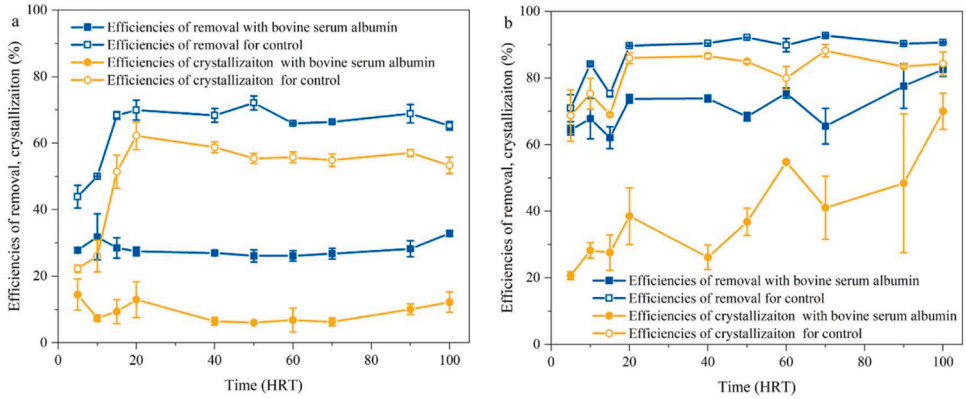

Fig. 6. Effects of bovine serum albumin on efficiencies of vivianite crystallization at pH 5.5 (a) and 6.5 (b).

Fe^{II} ion and activities of Fe^{II} and phosphate ions. As a result, the removal and recovery of PO_4-P from HTC liquor became less efficient. To eliminate the inhibition by proteins, it is suggested that pretreatments of sludge HTC liquor should be conducted in order to degrade proteins to monomers (with amino acids as the major components) prior to vivianite crystallization by either optimizing the HTC process or adding a treatment step for the HTC liquor.

3.4. Effects of pH on protein influences on vivianite crystallization

The level of pH plays a determinative role in the crystallization of vivianite because the speciation of both ferrous and phosphate ions and consequently the supersaturation are pH-dependent (Yang et al., 2023). With the pH increasing from 5.5 to 6.5, the efficiency of phosphorus removal and recovery increased significantly as expected (Figs. 1g and 6), while the inhibiting influence of BSA on vivianite crystallization remained although the extent of the inhibition seems to reduce slightly at high SIs (Fig. S6). This would exclude an explanation that the influence of BSA on vivianite crystallization was due to its surface charge, which is pH-regulated (Sah and Kundu, 2017). Compared with the difficulty in effectively retaining vivianite crystals in the reactor at pH 5.5, the continuous growth and accumulation of vivianite particles at pH 6.0 and 6.5 was found to reduce the inhibition of BSA on the crystallization (Figs. 1g and 6). The PSD curves and SEM images of the products obtained at pH 6.5 demonstrate that the increase in pH did not affect the growth mode of the vivianite crystals in the BSA-amended system addressed in Section 3.3 (Figs. S4, 5 and S7). The improved phosphorus removal at pH 6.5 increased the size of the products whilst the growth of vivianite crystals along the (020) plane was limited.

4. Conclusions

The influences of proteins in the HTC liquor of waste sewage sludge on vivianite crystallization for phosphorus recovery were discussed in this study. The freed sludge proteins during the carbonization treatment were mainly maintained in unhydrolyzed forms. The proteins could markedly decrease the efficiencies of vivianite crystallization in the HTC liquor whilst the components amino acids did not show similar influences. The inhibition of vivianite crystallization and the increase in the crystals size in the presence of proteins indicate that the Fe-protein interaction lowered the supersaturation level in the solution. The proteins also altered the mode of vivianite growth from spirally expanding to x/z axis-extending with the product morphology varying from being plate-like to radiating.

CRediT authorship contribution statement

Yue Zhang: Writing – review & editing, Writing – original draft, Methodology, Investigation, Conceptualization. **Xiaofan Yang:** Writing – review & editing, Methodology, Investigation. **Xinran Zhang:** Writing – review & editing, Methodology, Investigation. **Dezhi Sun:** Writing – review & editing, Methodology, Conceptualization. **Xinyi Liu:** Writing – review & editing, Methodology. **Rui Lan:** Writing – review & editing, Methodology. **Min Zheng:** Writing – review & editing, Methodology, Conceptualization. **Mark C.M. van Loosdrecht:** Writing – review & editing, Methodology, Conceptualization. **Xiang Cheng:** Writing – review & editing, Validation, Supervision, Project administration, Methodology, Investigation, Funding acquisition, Conceptualization.

Declaration of competing interest

The authors declare the following financial interests/personal relationships which may be considered as potential competing interests:

Xiang Cheng reports financial support was provided by Ministry of Science and Technology of the People's Republic of China. Xiang Cheng reports financial support was provided by National Natural Science Foundation of China. If there are other authors, they declare that they have no known competing financial interests or personal relationships that could have appeared to influence the work reported in this paper.

Data availability

Data will be made available on request.

Acknowledgments

This work was supported by the National Key Research and Development Program of China (no. 2021YFC3200604) and the Natural Science Foundation of China (nos. 52170023 and 51878048).

Supplementary materials

Supplementary material associated with this article can be found, in the online version, at doi:10.1016/j.resconrec.2024.107731.

References

Albetel, A.N., Outten, C.E., 2018. Characterization of glutaredoxin Fe-S cluster-binding interactions using circular dichroism spectroscopy. Methods Enzymol. 599, 327–353.

Aragón-Briceño, C.I., Pozarlik, A.K., Bramer, E.A., Niedzwiecki, L., Pawlak-Kruczek, H., Brem, G., 2021. Hydrothermal carbonization of wet biomass from nitrogen and phosphorus approach: a review. Renew. Energy 171, 401–415.

Brownlie, W.J., Sutton, M.A., Reay, D.S., Heal, K.V., Hermann, L., Kabbe, C., Spears, B. M., 2021. Global actions for a sustainable phosphorus future. Nat. Food 2 (2), 71–74.

Chen, X., Zheng, M., Cheng, X., Wang, C., Xu, K., 2022. Impact of impurities on vivianite crystallization for phosphate recovery from process water of hydrothermal carbonization of kitchen waste. Resour. Conserv. Recycl. 185, 106438.

Chiba, K., Takahashi, M., Ohshima, E., Kawamata, T., Sugiyama, K., 2020. The synthesis of metavivianite and the oxidation sequence of vivianite. J. Mineral. Petrol. Sci. 115 (6), 485–489.
Cordell, D., Drangert, J., White, S., 2009. The story of phosphorus: global food security and food for thought. Glob. Environ. Change 19 (2), 292–305.
Chrispim, M.C., Scholz, M., Nolasco, M.A., 2019. Phosphorus recovery from municipal wastewater treatment: critical review of challenges and opportunities for developing countries. J. Environ. Manag. 248, 109268.
Daugherty, E.E., Gilbert, B., Nico, P.S., Borch, T., 2017. Complexation and redox buffering of iron(II) by dissolved organic matter. Environ. Sci. Technol. 51 (19), 11096–11104.
Deng, S., Zhang, C., Dang, Y., Collins, R.N., Kinsela, A.S., Tian, J., Holmes, D.E., Li, H., Qiu, B., Cheng, X., Waite, T.D., 2020. Iron transformation and its role in phosphorus immobilization in a UCT-MBR with vivianite formation enhancement. Environ. Sci. Technol. 54 (19), 12539–12549.
Fukuzawa, K., Saitoh, Y., Akai, K., Kogure, K., Ueno, S., Tokumura, A., Otagiri, M., Shibata, A., 2005. Antioxidant effect of bovine serum albumin on membrane lipid peroxidation induced by iron chelate and superoxide. Biochim. Biophys. Acta-Biomembr. 1668 (1), 145–155.
Gächter, R., Müller, B., 2003. Why the phosphorus retention of lakes does not necessarily depend on the oxygen supply to their sediment surface. Limnol. Oceanogr. 48 (2), 929–933.
Hanzel, D., Melsel, W., Hanzel, D., GUtlich, P., 1990. Mössbauer effect study of the oxidation of vivianite. Solid State Commun. 3 (76), 307–310.
Huang, J., Wang, Z., Qiao, Y., Wang, B., Yu, Y., Xu, M., 2021. Transformation of nitrogen during hydrothermal carbonization of sewage sludge: effects of temperature and Na/Ca acetates addition. Proc. Combust. Inst. 38 (3), 4335–4344.
Huang, R., Fang, C., Lu, X., Jiang, R., Tang, Y., 2017. Transformation of phosphorus during (Hydro)thermal treatments of solid biowastes: reaction mechanisms and implications for P reclamation and recycling. Environ. Sci. Technol. 51 (18), 10284–10298.
Huang, R., Tang, Y., 2015. Speciation dynamics of phosphorus during (Hydro)thermal treatments of sewage sludge. Environ. Sci. Technol. 49 (24), 14466–14474.
Huang, R., Zhang, B., Saad, E.M., Ingall, E.D., Tang, Y., 2018. Speciation evolution of zinc and copper during pyrolysis and hydrothermal carbonization treatments of sewage sludges. Water Res. 132, 260–269.
Hung, K., Chang, Y., Eng, E.T., Chen, J., Chen, Y., Sun, Y., Hsiao, C., Dong, G., Spasov, K. A., Unger, V.M., Huang, T., 2010. Structural fold, conservation and Fe(II) binding of the intracellular domain of prokaryote FeoB. J. Struct. Biol. 170 (3), 501–512.
Karunanithi, R., Szogi, A.A., Bolan, N., Naidu, R., Loganathan, P., Hunt, P.G., Vanotti, M. B., Saint, C.P., Ok, Y.S., Krishnamoorthy, S., 2015. Chapter three: phosphorus recovery and reuse from waste streams. Adv. Agron. 131, 173.
Kelessidis, A., Stasinakis, A.S., 2012. Comparative study of the methods used for treatment and final disposal of sewage sludge in European countries. Waste Manag. 32 (6), 1186–1195.
Khalaf, N., Leahy, J.J., Kwapinski, W., 2023. Phosphorus recovery from hydrothermal carbonization of organic waste: a review. J. Chem. Technol. Biotechnol. 98 (10), 2365–2377.
King, J.E., Richards, J.E., Allerton, R., Wendt, R.H., 1983. Phosophorus removal in Ohio wastewater treatment plants within the Lake Erie basin. Ohio J. Sci. 83 (3), 91–96.
Lemos, V., Da Costa, M., Lemos, R., de Faria, M., 2007. Vivianite and siderite in lateritic iron crust: an example of bioreduction. Quim. Nova 30 (1), 36–40.
Li, C., Sheng, Y., 2021. Organic matter affects phosphorus recovery during vivianite crystallization. Water Sci. Technol. 83 (8), 2038–2050.
Li, Q., Liu, X., Hou, N., Wang, J., Wang, Y., Li, W., Chen, J., Mu, Y., 2022. Roles of humic acid on vivianite crystallization in heterogeneous nucleation for phosphorus recovery. J. Clean. Prod. 367, 133056.
Li, R., Cui, J., Li, X., Li, X., 2018. Phosphorus removal and recovery from wastewater using Fe-dosing bioreactor and cofermentation: investigation by X-ray absorption near-edge structure spectroscopy. Environ. Sci. Technol. 52 (24), 14119–14128.
Liu, H., Hu, G., Basar, I.A., Li, J., Lyczko, N., Nzihou, A., Eskicioglu, C., 2021. Phosphorus recovery from municipal sludge-derived ash and hydrochar through wet-chemical technology: a review towards sustainable waste management. Chem. Eng. J. 417, 129300.
Liu, J., Cheng, X., Qi, X., Li, N., Tian, J., Qiu, B., Xu, K., Qu, D., 2018. Recovery of phosphate from aqueous solutions via vivianite crystallization: thermodynamics and influence of pH. Chem. Eng. J. 349, 37–46.
Lowry, O.H., Rosebrough, N.J., Farr, A.L., Randall, R.J., 1951. Protein measurement with the folin phenol reagent. J. Biol. Chem. 193 (1), 265–275.
Lühmann, T., Wirth, B., 2020. Sewage sludge valorization via hydrothermal carbonization: optimizing dewaterability and phosphorus release. Energies 13 (17), 4417.
Mao, Y., Yang, S., Yue, Q., Wang, W., 2016. Theoretical and experimental study of the mechanisms of phosphate removal in the system containing Fe(III)-ions. Environ. Sci. Pollut. Res. 23 (23), 24265–24276.
Martin, N., Ya, V., Leewiboonsilp, N., Choo, K., Noophan, P.L., Li, C., 2020. Electrochemical crystallization for phosphate recovery from an electronic industry wastewater effluent using sacrificial iron anodes. J. Clean Prod. 276, 124234.
Mbughuni, M.M., Chakrabarti, M., Hayden, J.A., Bominaar, E.L., Hendrich, M.P., Munck, E., Lipscomb, J.D., 2010. Trapping and spectroscopic characterization of an FeIII-superoxo intermediate from a nonheme mononuclear iron-containing enzyme. Proc. Natl. Acad. Sci. USA 107 (39), 16788–16793.
Melton, E.D., Swanner, E.D., Behrens, S., Schmidt, C., Kappler, A., 2014. The interplay of microbially mediated and abiotic reactions in the biogeochemical Fe cycle. Nat. Rev. Microbiol. 12 (12), 797–808.
Mew, M.C., 2016. Phosphate rock costs, prices and resources interaction. Sci. Total Environ. 542, 1008–1012.
Miot, J., Benzerara, K., Morin, G., Bernard, S., Beyssac, O., Larquet, E., Kappler, A., Guyot, F., 2009. Transformation of vivianite by anaerobic nitrate-reducing iron-oxidizing bacteria. Geobiology 7 (3), 373–384.
Murphy, J.M., Powell, B.A., Brumaghim, J.L., 2020. Stability constants of bio-relevant, redox-active metals with amino acids: the challenges of weakly binding ligands. Coord. Chem. Rev. 412, 213253.
Ovsyannikova, E., Arauzo, P.J., Becker, G., Kruse, A., 2019. Experimental and thermodynamic studies of phosphate behavior during the hydrothermal carbonization of sewage sludge. Sci. Total Environ. 692, 147–156.
Pham, A.N., Waite, T.D., 2008. Oxygenation of Fe(II) in natural waters revisited: kinetic modeling approaches, rate constant estimation and the importance of various reaction pathways. Geochim. Cosmochim. Acta 72 (15), 3616–3630.
Pratt, A.R., 1997. Vivianite auto-oxidation. Phys. Chem. Miner. 25 (1), 24–27.
Priambodo, R., Shih, Y., Huang, Y., 2017. Phosphorus recovery as ferrous phosphate (vivianite) from wastewater produced in manufacture of thin film transistor-liquid crystal displays (TFT-LCD) by a fluidized bed crystallizer (FBC). RSC Adv. 7 (65), 40819–40828.
Prot, T., Korving, L., Dugulan, A.I., Goubitz, K., van Loosdrecht, M.C.M., 2021. Vivianite scaling in wastewater treatment plants: occurrence, formation mechanisms and mitigation solutions. Water Res 197, 117045.
Qiao, L., Xie, D., 2019. MIonSite: ligand-specific prediction of metal ion-binding sites via enhanced adaBoost algorithm with protein sequence information. Anal. Biochem. 566, 75–88.
Radisky, D.C., Kaplan, J., 1998. Iron in cytosolic ferritin can be recycled through lysosomal degradation in human fibroblasts. Biochem. J. 336 (1), 201–205.
Sah, B.K., Kundu, S., 2017. Modification of hysteresis behaviors of protein monolayer and the corresponding structures with the variation of protein surface charges. Colloids Surf. B 159, 696–704.
Senthilkumar, K., Mollier, A., Delmas, M., Pellerin, S., Nesme, T., 2014. Phosphorus recovery and recycling from waste: an appraisal based on a French case study. Resour. Conserv. Recycl. 87, 97–108.
Shi, Y., Luo, G., Rao, Y., Chen, H., Zhang, S., 2019. Hydrothermal conversion of dewatered sewage sludge: focusing on the transformation mechanism and recovery of phosphorus. Chemosphere 228, 619–628.
Steiner, G., Geissler, B., 2018. Sustainable mineral resource management—Insights into the case of phosphorus. Sustainability 10 (8), 2732.
Wang, L., Chang, Y., Li, A., 2019. Hydrothermal carbonization for energy-efficient processing of sewage sludge: a review. Renew. Sustain. Energy Rev. 108, 423–440.
Wang, Y., Zheng, K., Guo, H., Tong, Y., Zhu, T., Liu, Y., 2022. Unveiling the mechanisms of how vivianite affects anaerobic digestion of waste activated sludge. Bioresour. Technol. 343, 126045.
Wilfert, P., Mandalidis, A., Dugulan, A.I., Goubitz, K., Korving, L., Temmink, H., Witkamp, G.J., Van Loosdrecht, M.C.M., 2016. Vivianite as an important iron phosphate precipitate in sewage treatment plants. Water Res. 104, 449–460.
Wu, Y., Luo, J., Zhang, Q., Aleem, M., Fang, F., Xue, Z., Cao, J., 2019. Potentials and challenges of phosphorus recovery as vivianite from wastewater: a review. Chemosphere 226, 246–258.
Xu, Z., Ma, X., Zhou, J., Duan, P., Zhou, W., Ahmad, A., Luque, R., 2022. The influence of key reactions during hydrothermal carbonization of sewage sludge on aqueous phase properties: a review. J. Anal. Appl. Pyrolysis 167, 105678.
Xu, Z., Song, H., Li, P., He, Z., Wang, Q., Wang, K., Duan, P., 2020. Hydrothermal carbonization of sewage sludge: effect of aqueous phase recycling. Chem. Eng. J. 387, 123410.
Yang, G., Zhang, G., Wang, H., 2015. Current state of sludge production, management, treatment and disposal in China. Water Res. 78, 60–73.
Yang, X., Zhang, C., Zhang, X., Deng, S., Cheng, X., Waite, T.D., 2023. Phosphate recovery from aqueous solutions via vivianite crystallization: interference of Fe^{II} oxidation at different DO concentrations and pHs. Environ. Sci. Technol. 57 (5), 2105–2117.
Yu, B., Luo, J., Xie, H., Yang, H., Chen, S., Liu, J., Zhang, R., Li, Y., 2021. Species, fractions, and characterization of phosphorus in sewage sludge: a critical review from the perspective of recovery. Sci. Total Environ. 786, 147437.
Zhang, T., He, X., Deng, Y., Tsang, D.C.W., Jiang, R., Becker, G.C., Kruse, A., 2020. Phosphorus recovered from digestate by hydrothermal processes with struvite crystallization and its potential as a fertilizer. Sci. Total Environ. 698, 134240.